Compressible Flow Through Porous Media with Application to Injection

B. E. Schmidt

Internal Report for Caltech Hypersonics Group
FM 2014.001

California Institute of Technology, 1200 E California Blvd, Pasadena, CA 91125, USA

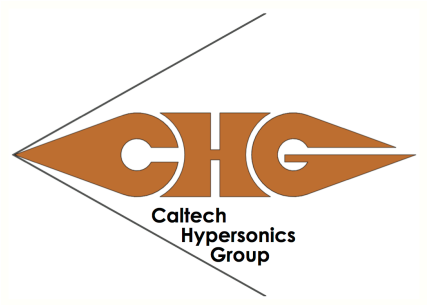

January 12, 2015

1 Introduction

Several sets of experiments have been performed in the last few years involving gaseous injection through porous metal injectors. These experiments require the mass flow rate of injected gas to be known, but it is not always measured directly. A theory relating the pressure difference across the injector to the mass flow rate through the injector is developed and verified in this document to calculate the mass flow rate of gas through one of the porous injectors used in these experiments.

2 Past Experiments

The first set of experiments involving injection were performed in T5 without careful consideration of the calculation of the mass flow rate. Carbon dioxide and argon were injected through a conical injector and into the hypersonic boundary layer on the 5-degree cone in T5. The effect on the location of boundary layer transition was examined. The mass flow rate was calculated based on measuring the pressure in a small tank feeding the injector assuming negligible losses through the tubing and valves. It has since been demonstrated that the initial calculations of mass flow rate were incorrect and they have been adjusted according to the theory developed in section 3.

A similar second set of experiments was performed in the Ludwieg Tube using both the conical injector used in the T5 experiments as well as a new cylindrical injector. Both injectors were purchased from Mott Corporation. The mass flow rate of the injected gas, here CO_2 and air, was measured directly using a Sensirion EM1 flow meter. Mass flow rates were found to be in the range of 0.5 to 3 g/s for the cylindrical injector and 0.5 to 1.5 g/s for the conical injector.

3 Compressible Darcy's Law

Darcy's Law for incompressible fluids is a well-known relation between flow rate and pressure difference for low-Reynold's number flows through porous media. The derivation is fairly simple and is based on conservation of momentum. The 1-D, steady equation has the form

$$Q = \frac{\kappa A}{\mu} \frac{P_1 - P_2}{L} \tag{1}$$

Here P_1 and P_2 are the pressures at the beginning and end of the media respectively, L is the length of the media, A is the area, μ is the viscosity of the fluid, and κ is the permeability of the porous media.

Shepherd et al has shown that 1-D steady flow through a porous media can be determined by the continuity equation and the force balance between drag and the pressure drop across an element of porous material [1].

$$\frac{\partial \rho u}{\partial x} = 0 \tag{2}$$

$$-\frac{\partial p}{\partial x} = \frac{\rho u^2}{\bar{d}} C_D(Re, \epsilon, \bar{d}) \tag{3}$$

Here $\bar{d}$ is a mean particle size for the porous material. If the material is approximated as a bed of packed spheres, then $\bar{d}$ is the diameter of the spheres. ϵ is the porosity (volume fraction of pore space) of the material and Re is the Reynolds number based on $\bar{d}$, i.e. $Re = \rho u \bar{d}/\mu$. Equation 2 simplifies to $\dot{m} = \rho u =$ constant, which means that Re is also a constant. Thus the momentum equation can be written

$$-\rho \frac{\partial p}{\partial x} = \frac{\dot{m}^2}{\bar{d}} C_D = \text{constant} \tag{4}$$

Using the ideal gas law $p = \rho RT$ and assuming that the gas is isothermal through the porous material allows the equation to be integrated directly from 0 to L to give

$$P_0^2 - P_a^2 = 2RT\dot{m}^2 C_D \frac{L}{\bar{d}} \tag{5}$$

3.1 Drag Coefficient

An expression is still needed for the drag coefficient C_D of the porous material in order to use Equation 5. Because of the low Reynolds number in flow through porous media, the Forchheimer equation can be used to approximate a drag coefficient of the form

$$C_D = \frac{\bar{d}^2}{\kappa}\left(\frac{1}{Re} + \frac{\lambda}{\bar{d}}\right) \tag{6}$$

κ is again the permeability of the material and λ is the Forchheimer constant, which is related to the permeability but must be determined experimentally. Substituting the appropriate expression for the Reynolds number, Equation 6 becomes

$$C_D = \frac{\bar{d}}{\kappa}\left(\frac{\mu}{\dot{m}} + \lambda\right) \tag{7}$$

λ can then be expressed in terms of $\bar{d}$ and ϵ using the Carman-Kozeny expression for the permeability

$$\kappa = \frac{\bar{d}^2\epsilon^3}{180(1-\epsilon)^2} \tag{8}$$

and the Ergun relation for the Forchheimer constant

$$\frac{\kappa}{\lambda} = \frac{\bar{d}\epsilon^3}{1.8(1-\epsilon)} \tag{9}$$

Both of these equations approximate the porous material to be made from packed spherical particles with a surface-averaged particle diameter of $\bar{d}$. κ can be eliminated from these two equations to yield

$$\lambda = \frac{\bar{d}}{100(1-\epsilon)} \tag{10}$$

This is substituted into Equation 7 to give

$$C_D = \frac{\bar{d}}{\kappa}\left(\frac{\mu}{\dot{m}} + \frac{\bar{d}}{100(1-\epsilon)}\right) \tag{11}$$

3.2 Application to Injectors

The conical and cylindrical injectors used in the experiments described in Section 2 are shown in Figure 1. Because the half-angle of the conical injector is small, it can be approximated as cylindrical using an average radius for the purposes of modeling. With this approach, the cylindrical injector has a length of 35 mm an outer radius of 11.1 mm, and an inner radius of 7.93 mm. The conical injector is 40 mm long with a mean outer radius of 13.3 mm and a mean inner radius of 11.72 mm.

The permeability κ of the injectors is not known *a priori*, it must be determined experimentally. Estimates can be made using Equation 8 to confirm that the measurement is reasonable within an order of magnitude. According to Mott Corporation, ϵ is approximately equal to 0.4 for sintered steel and $\bar{d}$ is on the order of 10 μm. This value for $\bar{d}$ appears to be reasonable for the cylindrical injector using Figure 2 as a reference, but the conical injector clearly has a smaller characteristic particle size, perhaps by one order of magnitude. Assuming a mean particle diameter of 10 μm yields a rough estimate of κ of 10^{-13} m^2 with an uncertainty of slightly more than an order of magnitude to account for the large uncertainty in $\bar{d}$.

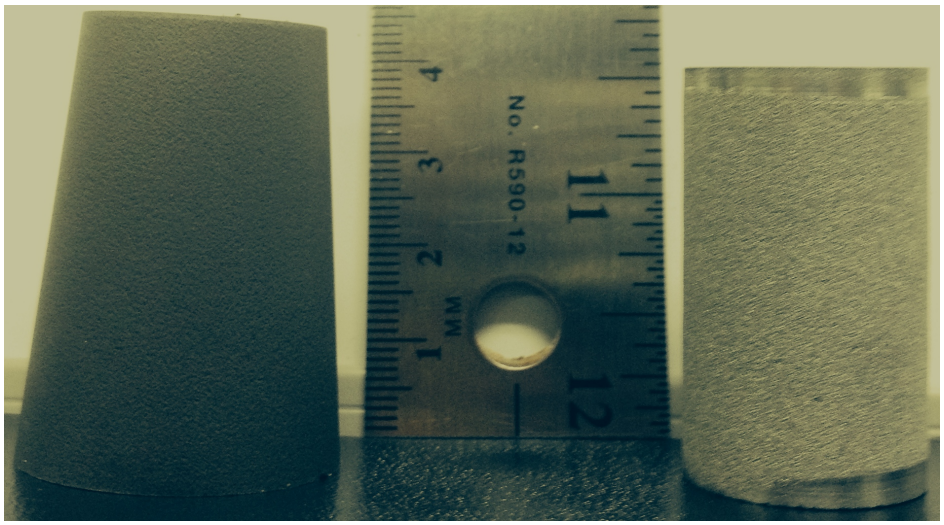

Figure 1: Conical and cylindrical injectors used in experiments.

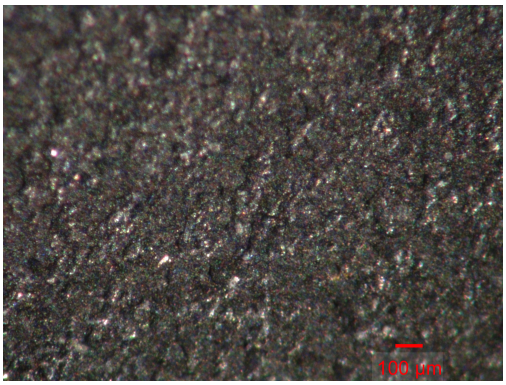

(a) Conical injector surface under 5x magnification. Line in lower right shows scale

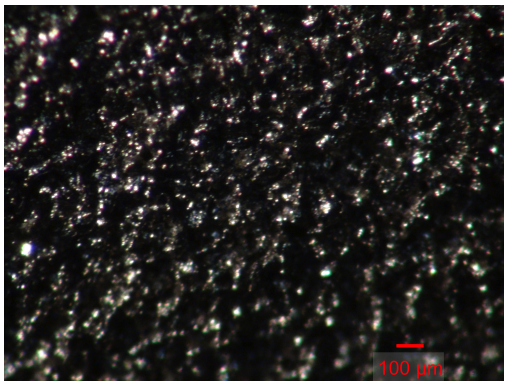

(b) Cylindrical injector surface under 5x magnification. Line in lower right shows scale

Figure 2: Injector surfaces under magnification.

Using these values, the two terms in Equation 11 can be compared for the experiments performed. The viscosity of air at room temperature is 1.9×10^{-5} kg/m s, and the viscosity of carbon dioxide is 7.0×10^{-5} kg/m s. Assuming the smaller value of the two for viscosity, the largest mass flow rate measured of 0.0045 kg/s divided by an effecitve injector area of approximately 1 $\times 10^{-3}$ m^2, and a characteristic particle size of 10 μm, the first term in Equation 11, $\mu/\dot{m}$, is on the order of 4.2 μm while the second term is approximately 0.2 μm. Thus the second term is at most 4.7% of the first term and can be neglected. This simplifies the expression for the drag coefficient significantly to

$$C_D = \frac{\bar{d}\mu}{\kappa \dot{m}} = \frac{\bar{d}^2}{\kappa} \frac{1}{Re} \tag{12}$$

One further step is required. Equation 5 is for one-dimensional flow, but a similar expression can be derived for axisymmetric flow. The continuity equation is

$$\frac{d}{dr}(\rho u) + \frac{\rho u}{r} = 0 \tag{13}$$

which reduces to

$$\rho u r = \text{constant} = \frac{\dot{m}}{2\pi L} \tag{14}$$

for a cylinder of length L. The momentum equation is very similar to Equation 3 except with a derivative taken in r instead of x because there is still a balance between the pressure difference across the injector and a drag inside the injector.

$$-\frac{dp}{dr} = \frac{\rho u^2 C_D}{\bar{d}} \tag{15}$$

The Forchheimer expression for the drag coefficient is still valid because it is only a function of Reynolds number and the material properties of the injector. This can be substituted into the momentum equation to give

$$-\frac{dp}{dr} = \frac{u\mu}{\kappa} \tag{16}$$

The velocity u can be expressed in terms of the mass flow rate using Equation 14.

$$-\rho\frac{dp}{dr} = \frac{\dot{m}\mu}{2\pi L\kappa r} \tag{17}$$

Using the ideal gas law to express ρ as a function of p and assuming that the gas is isothermal through the injector, this equation can be integrated from P_0 to P_a in p and from R_i to R_o in r to yield

$$P_0^2 - P_a^2 = \frac{\dot{m}\mu RT}{\pi L\kappa}\ln\left(\frac{R_o}{R_i}\right) \tag{18}$$

By rewriting the logarithm as $\ln(1 + h/R_i)$ where h is the thickness of the injector and expanding in a Taylor series, the logarithm term is equal to h/R_i to first order. By substituting this into equation 18 and recognizing that $\dot{m}$ in that equation is $\dot{m}$ in equation 5 times the effective area of the injector, one recognizes that the two equations are identical.

In the experiments performed, the ambient pressure outside the injector is quite low, so $P_a^2/P_0^2 << 1$ and Equation 18 can be approximated as

$$P_0^2 = \frac{\dot{m}\mu RT}{\pi L\kappa}\ln\left(\frac{R_o}{R_i}\right) \tag{19}$$

The validity of this assumption will be investigated in Section 4.

4 Model Verification

4.1 Experiments

A set of experiments were performed to simultaneously measure pressure inside the injector and the gas mass flow rate. A measurement unit fitted with a Kulite XT-190 piezoresistive pressure transducer was attached to the injector instead of the cone tip used in experiments. The apparatus was positioned inside the test section of the Ludwieg tube as it would be for an experiment in supersonic flow, but no flow was produced. The chamber was evacuated to a partial vacuum to the edge pressure that would be outside the injector during an experiment, approximately 2.7 kPa. This value was determined using the Taylor-Maccoll solution for supersonic flow over a cone. Gas was then allowed to flow through the injector and the mass flow rate and pressure were measured simultaneously at various mass flow rates. These experiments were performed with both air and carbon dioxide with both the conical and cylindrical injectors.

Sample mass flow rate and pressure data are shown in Figures 3 and 4 respectively. The raw data was filtered with a second-order Butterworth filter to eliminate electrical noise due to the connection through a

feedthrough plate. Averaging windows were selected for the mass flow rate and the pressure once steady-state was reached. The average value for each is tabulated for all experiments performed and those values are plotted against each other in Figures 5 through 8. Limits on maximum pressure arise in each experiment from the regulators used on the injection fill bottles and pressure losses in the flow path from the fill bottle to the injector.

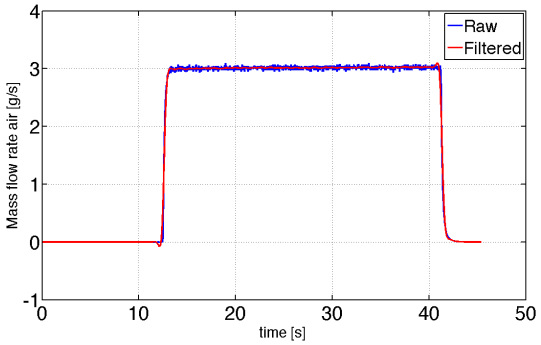

Figure 3: Example experimental data for mass flow rate for air with the cylindrical injector (Shot 181)

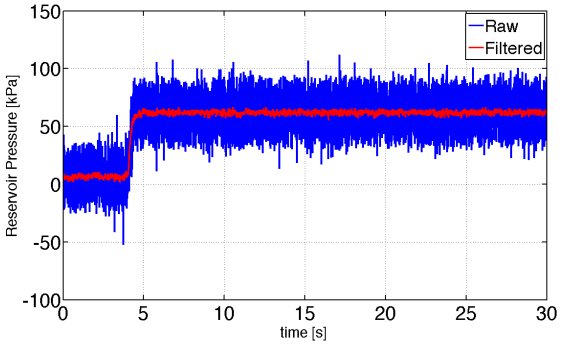

Figure 4: Corresponding pressure data for Shot 181. The times in the mass flow rate and pressure data do not correspond directly because the pressure transducer and flow meter are triggered at separate times during data acquisition.

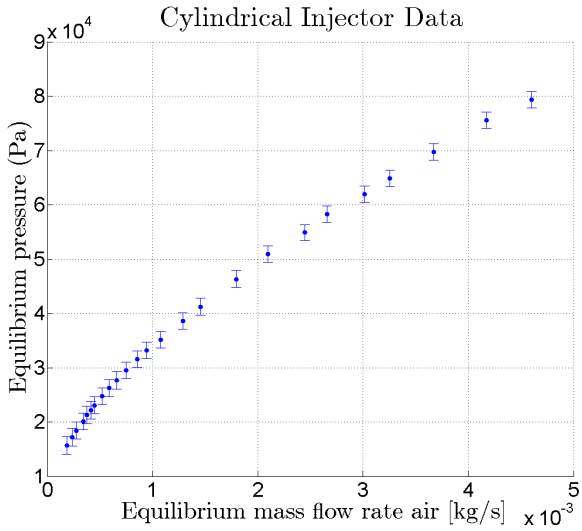

Figure 5: Pressure vs. Mass flow rate data for air with the cylindrical injector. Uncertainty in mass flow rate is negligible compared to uncertainty in pressure.

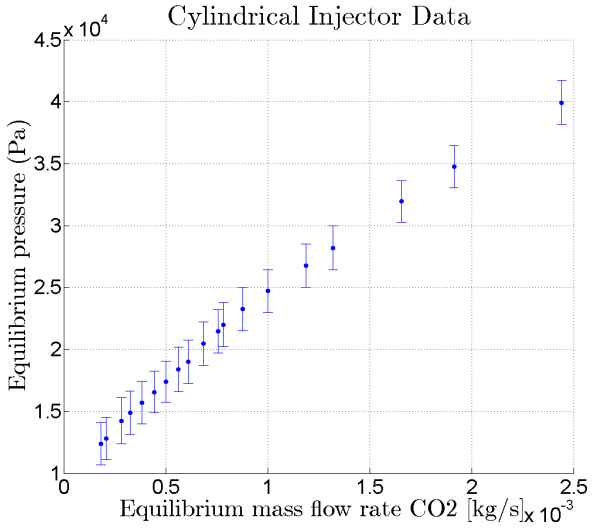

Figure 6: Pressure vs. Mass flow rate data for carbon dioxide with the cylindrical injector.

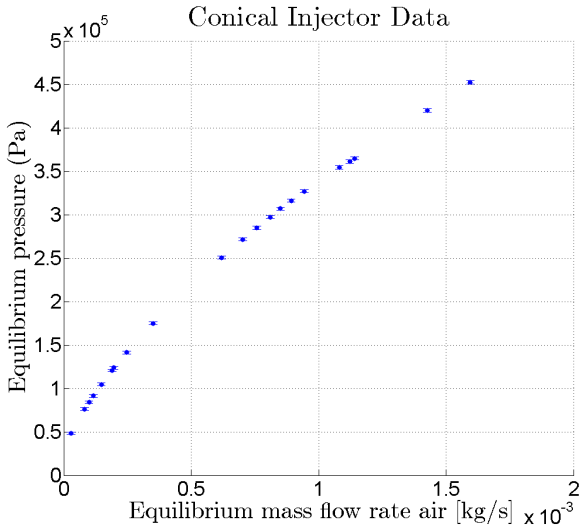

Figure 7: Pressure vs. Mass flow rate data for air with the conical injector.

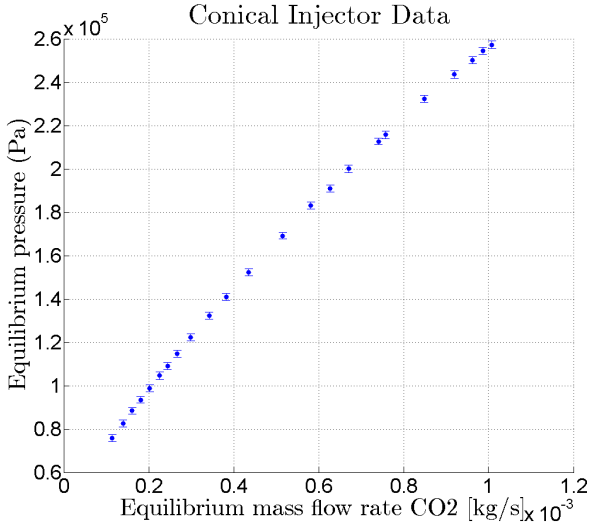

Figure 8: Pressure vs. Mass flow rate data for carbon dioxide with the conical injector.

In order to confirm the validity of Equation 19, the data sets are fitted to square-root curves using linear least-squares by casting the relationship between pressure and the square root of the mass flow rate. In this case, the slope is determined by the product of the coefficients in Equation 19 with the only unknown coefficient being the permeability κ. Allowing the slope of the best-fit line to be a free parameter allows κ to be calculated. The y-intercept of the best-fit line is also allowed to be a free parameter in order to obtain the best possible fit because although Equation 19 predicts that the mass flow rate will be zero when the pressure is zero, the square-root relationship is expected to break down at very low flow rates as the flow enters the non-continuum regime [1]. The ambient pressure will also become important at low pressures and flow rates. In all cases the 95% confidence interval for the y-intercept is of the same order as the magnitude of the y-intercept itself and exceeds it in one case, so a nonzero y-intercept in the least-squares fit is not significant in these calculations.

Figures 9 through 12 show the data sets with their respective least-squares fits and the calculated values

of κ. The values for κ agree within 25% for the cylindrical injector and within 4% for the conical injector. The fit for air injection in the cylindrical injector is considered to be better as it passes through a larger portion of the parameter space. Uncertainty in κ is calculated to be a quadrature sum of the uncertainty based on the 95% confidence interval based on the curve fit and the uncertainty propagated from the uncertainty in pressure. The excellent quality of the fits in all cases lends significant credibility to the analysis in Section 3. It is also reassuring that the calculated values of κ are reasonable according to Equation 8.

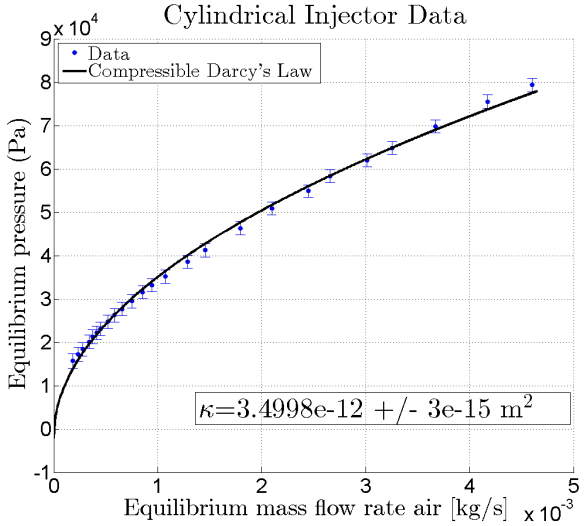

Figure 9: Pressure vs. Mass flow rate data for air with the cylindrical injector fit with Equation 19 to determine permeability.

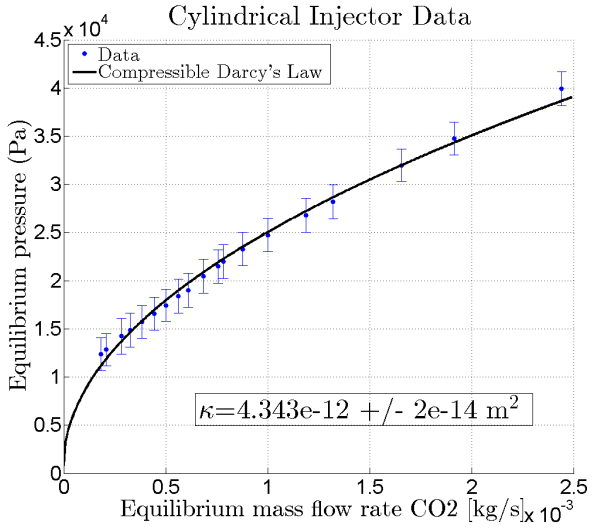

Figure 10: Pressure vs. Mass flow rate data for carbon dioxide with the cylindrical injector fit with Equation 19 to determine permeability.

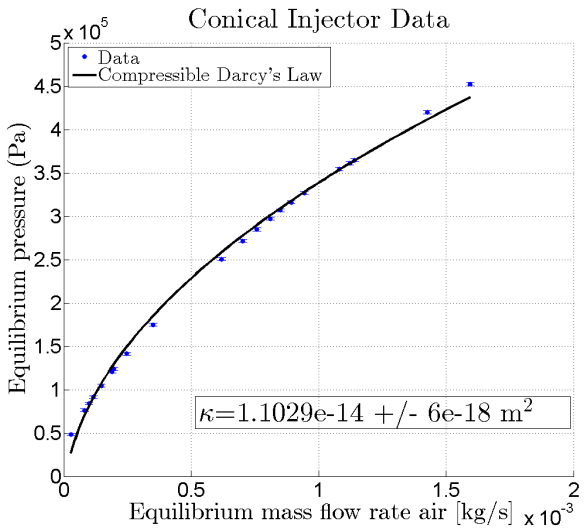

Figure 11: Pressure vs. Mass flow rate data for air with the conical injector fit with Equation 19 to determine permeability.

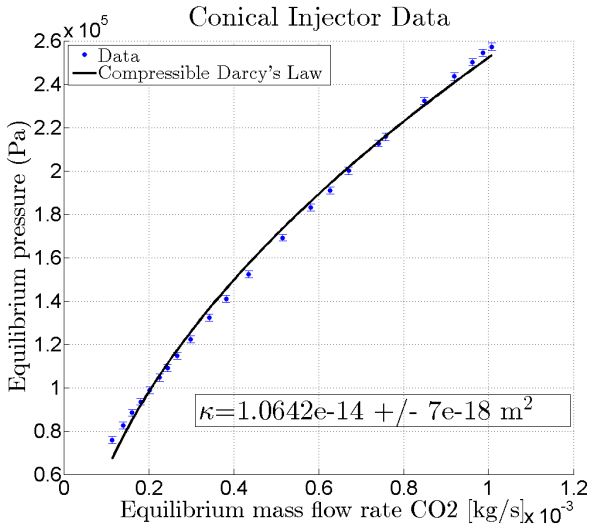

Figure 12: Pressure vs. Mass flow rate data for carbon dioxide with the conical injector fit with Equation 19 to determine permeability.

4.2 Inclusion of Inertial Term

Because the inertial term in the momentum equation is ignored in the derivation of Equation 19, the effects of choking are not considered. In order to account for this effect, one could think of the injectors as being made up of an array of very small tubes which could then be analyzed using one-dimensional, frictional, compressible flow. The flow can be approximated either as isothermal or adiabatic, but for low Mach numbers there is little difference between the two. Thus adiabatic flow will be analyzed because it simplifies calculations. The equations for one-dimensional, steady, frictional, compressible, adiabatic flow are the familiar Fanno flow equations. The choking condition for Fanno flow is $M = 1$ at the exit of the duct. Two of the Fanno flow equations are needed to determine the pressure-mass flow relation. A one-dimensional analysis will be performed here to simplify calculations. When the flow is choked, the following equations may be written.

$$4C_f \frac{L}{D} = \frac{1 - M^2}{\gamma M^2} + \frac{\gamma + 1}{2\gamma} \log \frac{(\gamma + 1)M^2}{2\left(1 + \frac{\gamma - 1}{2} M^2\right)} \tag{20}$$

$$\frac{P_0}{P_a} = \frac{1}{M} \sqrt{\frac{\gamma + 1}{2\left(1 + \frac{\gamma - 1}{2} M^2\right)}} \tag{21}$$

Here C_f is related to C_D used in the simplified model, specifically $2C_f = C_D$. The parameter $4C_f \frac{L}{D}$ is important, it will be shortened to $\bar{L}$, the normalized duct length. $\bar{L}$ is related to the mass flow rate by the definition of C_D:

$$\dot{m} = \frac{2L\mu A}{\bar{L}\kappa} \tag{22}$$

If the flow is not choked, a simple method exists to determine exit conditions using Equations 20 and 21. These equations can be solved numerically when they are parameterized by M^2, the Mach number at the entrance to the injector squared for both subsonic and choked conditions. Figure 13 shows the pressure-mass flow relation from Fanno flow.

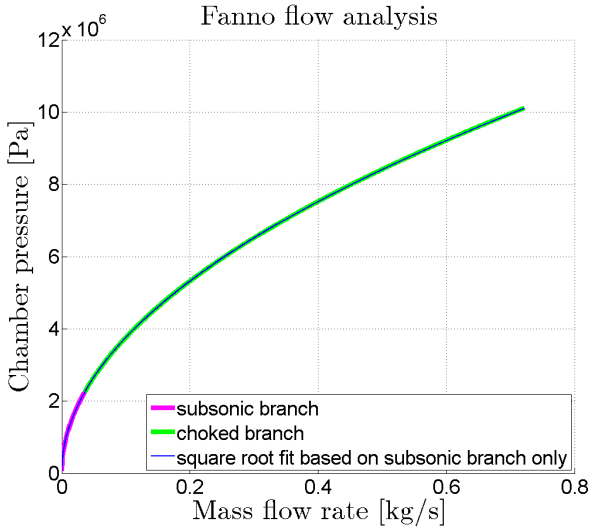

Figure 13: Pressure vs. Mass flow rate for Fanno flow analysis using parameters based on air in the conical injector. Note that the blue curve representing the square root fit of the pink subsonic branch perfectly coincides with the green choked branch.

Figure 13 demonstrates that choking has no effect on the relationship between pressure and mass flow rate, and the same square root relationship at low Mach numbers is valid under choked conditions as well. Figure 13 is not meant to be quantitative, it simply demonstrates the qualitative impact of choking on the pressure vs. mass flow rate relation for porous media. This lends additional confidence to the analysis in Section 3.

In addition to the preceding analysis, it is also possible to calculate the maximum Mach number encountered in experiments in order to determine if the flow is indeed choked. With the ideal gas law and some algebra, the Mach number can be written as

$$M = \frac{\rho u}{p}\sqrt{\frac{RT}{\gamma}} \tag{23}$$

Here the pressure p is the pressure at the exit of the injector, which is 2700 Pa, and the temperature is likewise the temperature at the exit of the injector. Treating the flow through the injector as adiabatic, the temperature is a function of Mach number.

$$T = T_0(1 + \frac{\gamma - 1}{2}M^2)^{-1} \tag{24}$$

An equation for the exit Mach number can then be written using the stagnation temperature.

$$M = \left(\frac{-1 + \sqrt{1 + 2(\gamma - 1)\frac{\dot{m}}{AP_a}\sqrt{\frac{RT_0}{\gamma}}}}{\gamma - 1}\right)^{\frac{1}{2}} \tag{25}$$

From this equation it is clear that air will produce a higher exit Mach number than carbon dioxide. The maximum flow rate for the conical injector is 1.6×10^{-3} kg/s, which corresponds to an exit Mach number of 0.15. Likewise the maximum flow rate for the cylindrical injector is 4.6×10^{-3} kg/s, corresponding to an exit Mach number of 0.41. Thus the maximum Mach number encountered in these experiments is 0.41. Additionally this demonstrates that the temperature of the gas in the injector changes by at most 3.3%, validating the isothermal assumption made in Section 3.

4.3 Inclusion of Forchheimer Term to Drag Coefficient

The calculation of the permeability κ for each injector in Section 4.1 allows the mean particle diameter $\bar{d}$ to be estimated more accurately by the Carman-Kozeny equation (Equation 8). This in turn allows a more relevant comparison of the two terms in the drag coefficient can be made. The mean particle diameter for the conical injector is 3.3 μm, and for the cylindrical injector it is 64 μm assuming a value of 4×10^{-12} m^2 for κ. Therefore the second term in Equation 11, the Forchheimer Term, has a value of 0.055 μm for the conical injector and 1.1 μm for the cylindrical injector. The Forchheimer Term is clearly still insignificant for the conical injector, less than 1% of the first term. For the cylindrical injector, however, the Forchheimer term can be up to 25% of the first term in the Carman-Kozeny equation, so it should be retained.

Returning to Equation 15 and substituting for the drag coefficient, the equation becomes

$$-\frac{dp}{dr} = \frac{\rho u^2}{\kappa}\left(\frac{\mu}{\rho u} + \frac{\bar{d}}{100(1 - \epsilon)}\right) \tag{26}$$

After some algebra and substituting for $\bar{d}$ using Equation 8 this becomes

$$-\rho\frac{dp}{dr} = \frac{\dot{m}\mu}{2\pi L\kappa r} + \frac{3\sqrt{5}}{50\sqrt{\kappa}\epsilon^{\frac{3}{2}}}\left(\frac{\dot{m}}{2\pi Lr}\right)^2 \tag{27}$$

This equation can be integrated from the inside of the injector to the outside with an isothermal assumption to give

$$P_0^2 - P_a^2 = \frac{RT}{2\pi L}\left(\frac{\dot{m}\mu}{\kappa}\ln\left(\frac{R_o}{R_i}\right) + \frac{3\sqrt{5}\dot{m}^2}{100\epsilon^{-\frac{3}{2}}\sqrt{\kappa}\pi L}\left(\frac{1}{R_i}+\frac{1}{R_o}\right)\right) \tag{28}$$

P_a can again be neglected in favor of P_0 for the experiments performed in this study. The permeability can no longer be determined by linear least squares because Equation 28 can no longer be linearized in terms of κ. It is still possible, however, to determine a value for κ by minimizing the total error in the least-squares sense. The error in one measurement is given by

$$\sigma_i = \frac{RT}{2\pi L}\left(\frac{\dot{m}_i\mu}{\kappa}\ln\left(\frac{R_o}{R_i}\right) + \frac{3\sqrt{5}\dot{m}_i^2}{100\epsilon^{-\frac{3}{2}}\sqrt{\kappa}\pi L}\left(\frac{1}{R_i}+\frac{1}{R_o}\right)\right) + b - P_{0_i}^2 \tag{29}$$

Thus the total error is the quadrature sum of the errors in each measurement, i.e.

$$E = \|\underline{\sigma}\|_2 = \left(\sum_{i=1}^{n}\sigma_i^2\right)^{\frac{1}{2}} \tag{30}$$

In the case of fitting κ and b such that the total error is minimized, $E = E(\kappa, b)$. Thus the minimum error occurs when

$$\frac{\partial E}{\partial \kappa} = \frac{\partial E}{\partial b} = 0$$

Thus the two equations to be solved are

$$\sum_{i=1}^{n}\sigma_i(\kappa,b)\frac{\partial\sigma_i}{\partial\kappa} = 0 \text{ and } \sum_{i=1}^{n}\sigma_i(\kappa,b)\frac{\partial\sigma_i}{\partial b} = 0$$

From Equation 29 it is clear that $\partial\sigma_i/\partial b = 1$ for all i. This allows the parameter b to be determined explicitly in terms of κ as follows.

$$b = \frac{1}{n}\left[\sum_{i=1}^{n}P_{0_i}^2 - \frac{RT}{2\pi L}\sum_{i=1}^{n}\left(\frac{\dot{m}_i\mu}{\kappa}\ln\left(\frac{R_o}{R_i}\right) + \frac{3\sqrt{5}\dot{m}_i^2}{100\epsilon^{-\frac{3}{2}}\sqrt{\kappa}\pi L}\left(\frac{1}{R_i}+\frac{1}{R_o}\right)\right)\right] \tag{31}$$

This expression is substituted into the expression for $\partial E/\partial\kappa$ to obtain an equation for κ that minimizes the total error. The partial derivative of σ_i with respect to κ must also be evaluated. It is

$$\frac{RT}{2\pi L}\left(-\frac{\dot{m}\mu}{\kappa^2}\ln\left(\frac{R_o}{R_i}\right) - \frac{3\sqrt{5}\dot{m}^2}{200\epsilon^{\frac{3}{2}}\kappa^{\frac{3}{2}}\pi L}\left(\frac{1}{R_i}-\frac{1}{R_o}\right)\right) \tag{32}$$

The resulting equation for κ must be solved numerically, and the resulting value for κ is substituted into Equation 31 to obtain a corresponding value for b. This is done for both experimental cases with the cylindrical injector. The resulting curves and values for κ shown in Figures 14 and 15. There is a small but noticeable qualitative improvement in the fit when including the Forchheimer term, especially at higher flow rates where the Forchheimer term would become more significant. The total error is increased by 10% in the case of air but decreased by 13% in the case of carbon dioxide, so there is only a small net quantitative improvement where error is concerned. The most important improvement, however, is the close agreement in the values of κ obtained by including the Forchheimer term in the drag coefficient (11%) when the values were previously quite different (20%).

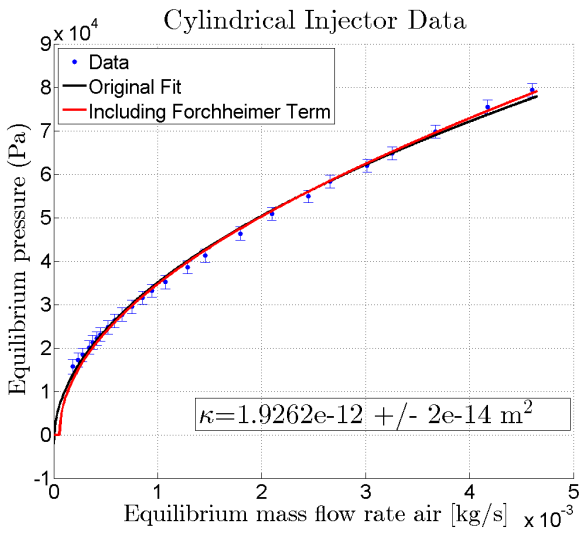

Figure 14: Pressure vs. Mass flow rate data for air with the cylindrical injector fit with Equation 19 (black) and Equation 28 (red) to determine permeability.

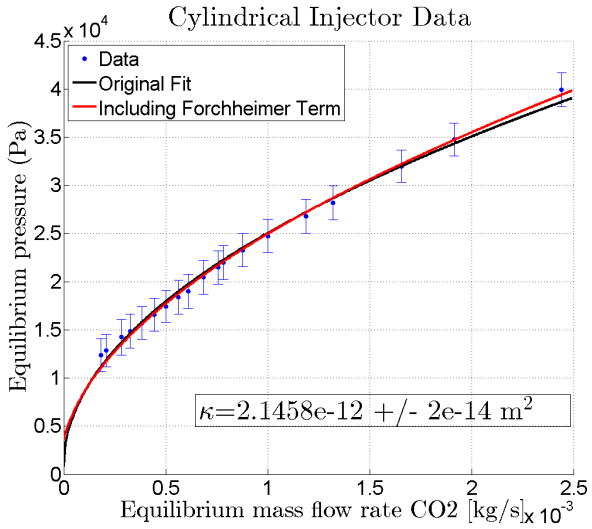

Figure 15: Pressure vs. Mass flow rate data for carbon dioxide with the cylindrical injector fit with Equation 19 (black) and Equation 28 (red) to determine permeability.

4.4 Knudsen number considerations

As a final examination of assumptions, it is worthwhile to consider the range of Knudsen numbers encountered in the experiments and determine if the continuum assumption remains valid. The Knudsen number is defined as the mean free path of the molecules in the fluid divided by a characteristic length scale of the flow, $Kn = \lambda/L$. If the Knudsen number is greater than or equal to one, the flow is rarefied and the continuum assumption no longer holds. There is also a transitional region for Knudsen number slightly less than one where the continuum assumption begins to break down.

It is often convenient, as in this case, to relate the Knudsen number to the Mach number. This is a fairly straightforward and well-known conversion based on the definitions of the three numbers and the calculation

of the mean free path for an ideal gas. The steps will be skipped here and only the final result is reported.

$$Kn = \frac{M}{Re}\sqrt{\frac{\gamma\pi}{2}} \tag{33}$$

Using the formulation of the Mach number in Equation 23, the Kudsen number can be written as

$$Kn = \sqrt{\frac{RT\pi}{2}}\frac{\mu}{p\bar{d}} \tag{34}$$

From this formulation, it is clear that the Knudsen number will be higher for carbon dioxide flow than air flow because of viscosity and will then only vary with pressure. The Knudsen number will be highest when the pressure is at its lowest, which is at the injector exit. Numerically, using values for carbon dioxide, the Knudsen number is $6225/p$ for the conical injector and $462/p$ for the cylindrical injector (p in Pascals). Thus for an exit pressure of 2.7 kPa the flow is most likely transitional or even free-molecular at the injector exit but in the continuum regime throughout at least 95% of the thickness of the injector assuming a linear pressure drop. The maximum Knudsen number at the injector entrance encountered for the cylindrical injector is 0.03, safely inside the continuum regime, but the maximum Knudsen number at the entrance for the conical injector is 0.10 because of the much smaller permeability. A Knudsen number of 0.10 is not entirely in the continuum regime, but is beginning to enter the transitional flow regime. This may account for a very small amount of misfit near the low flow rate points in Figure 12, but these are the only points for which a Knudsen number effect is important and the effect (if any) does not appear to be significant. It should be noted, however, that the models developed here should not be extrapolated to much lower chamber pressures than the ones enumerated in the report because of the onset of transitional and rarefied flow.

5 Conclusion

A simple equation to relate mass flow rate to internal pressure for steady gas flow through a porous injector is derived and validated by experiments and a more complete analysis. The equation predicts a square-root dependence of pressure on mass flow rate with one free parameter for a given injector, the permeability. This allows the permeability to be measured for a given injector if the mass flow rate and pressure are measured independently by fitting a curve to the data. This was done for injectors used for experiments in the Ludwieg Tube and T5.

References

[1] J. E. Shepherd and D. R. Begeal. Transient compressible flow in porous materials. Technical Report SAND-83-1788, Sandia National Labs, Albuquerque, NM (USA), 1988.